

Structured air lasing of N_2^+

Jingsong Gao ¹, Xiang Zhang², Yang Wang ¹, Yiqi Fang¹, Qi Lu², Zheng Li ¹, Yi Liu ^{2,3}✉, Chengyin Wu¹, Qihuang Gong ¹, Yunquan Liu ¹✉ & Hongbing Jiang ¹✉

Air lasing is a simple and promising technique to efficiently produce coherent light in the atmosphere. Yet, its capability to obtain structured light like optical vortices or vector beams is still unexplored. Here, we demonstrate the generation of vortex superfluorescent radiation with the same orbital angular momentum as the pump beam, obtained via N_2^+ lasing by focusing a vortex pump beam on N_2 gas. The vortex superfluorescence is amplified without altering the vorticity when seeded by a Gaussian beam, in which the vortex pump beam transfers the spatial spiral phase into the N_2^+ gain medium and the N_2^+ lasing obtains the phase information. The same mechanism is applied for a vector pump beam, turning the Gaussian seed into an amplified cylindrical vector beam. We corroborate our mechanism for generating vectorially structured light via air lasing with numerical calculations. This work provides a promising approach to generating structured light via superfluorescence.

¹State Key Laboratory for Mesoscopic Physics, School of Physics, Peking University, Beijing 100871, China. ²Shanghai Key Lab of Modern Optical System, University of Shanghai for Science and Technology, Shanghai 200093, China. ³CAS Center for Excellence in Ultra-intense Laser Science, Shanghai 201800, China. ✉email: yi.liu@usst.edu.cn; yunquan.liu@pku.edu.cn; hbjiang@pku.edu.cn

With the development of emerging laser sculpting techniques, the amplitude, phase and polarization of the fundamental Gaussian laser mode can be completely controlled, giving rise to many interesting spatiotemporal modes^{1,2}, such as optical vortices (OVs)³ and vector beams (VBs)⁴. An OV is a light field with a spatially spiral phase structure and intrinsic photon orbital angular momentum (OAM), and it is typically described by a Laguerre-Gaussian (LG) mode⁵. Because the OAM of a photon is multiple-valued, it provides a highly dimensional degree of freedom for applications in many fields, such as super-resolution microscopy⁶, optical tweezers^{7,8}, spinning object detection⁹, and high-capacity optical communication via OAM multiplexing^{10,11}. In contrast, a VB is a light field with a spatially varying state of polarization. One paradigm of VBs is cylindrical vector beams (CVBs), which exhibits cylindrically symmetric polarization⁴. Owing to their unique dynamic properties, CVBs have attracted broad interest in various scientific communities, ranging from optical trapping¹² and high-resolution imaging^{13,14} to communications^{15,16} and quantum memory¹⁷. In particular, cylindrical vector vortex beams, that is, CVBs carrying OAM, have recently been used to study the spin-orbit interaction of light^{18,19}. The generation of OVs and CVBs conventionally relies on linear optical processes and photonic devices that directly convert a Gaussian beam into a structured light beam, such as spiral phase plates (SPPs)²⁰, spatially variant half-wave plates (SWPs, half-wave q-plates)²¹, and spatial light modulators^{22,23}. Alternatively, structured light can also be launched from lasers²⁴, in which special optical elements are placed in the laser cavity to produce the desired modes. Recently, nonlinear intense light-matter interactions have propelled the generation of structured light fields with an extensive wavelength range²⁵. For example, one can employ high harmonic generation (HHG) to create extreme ultraviolet OVs^{26,27} and CVBs²⁸, and simultaneously control the spin-orbit state of extreme ultraviolet photons²⁹. Indeed, it is worthwhile to seek new generation routines of structured light fields using light-matter interactions, which would provide not only a robust and promising toolbox for complete control over structured light fields but also a promising way to discover new physical phenomena.

Air lasing is a cavity-free lasing action that is generated in air owing to the plasma filamentation process of high-power femtosecond laser pulses^{30,31}. In particular, the coherent emission of N_2^+ at 391 nm pumped by femtosecond laser pulses at 800 nm has gained increasing attention due to its rich physical mechanism^{32–41}. It is now generally accepted that the coherent emission of N_2^+ at 391 nm is essentially superfluorescence^{39,40}, which is a distinctive quantum optics phenomenon^{42–44} and is collectively emitted from a macroscopic dipole⁴⁵. If an external seed light with a spectrum covering 391 nm is injected into the plasma, the coherent emission of N_2^+ at 391 nm will be amplified by several orders of magnitude⁴⁰. Many studies on enhancing the intensity of N_2^+ air lasing are ongoing^{46,47}. However, laser beams with space-variant phases or polarizations, that is, OVs or VBs, have not yet been applied to N_2^+ air lasing.

Here, we report a physical mechanism that enables the amplification of a Gaussian seed beam into structured light via N_2^+ air lasing. Spatially structured light is first employed to drive N_2^+ air lasing. By focusing a p -polarized vortex pump beam at 800 nm on N_2 gas, we generate a vortex signal of N_2^+ air lasing at 391 nm with the same OAM as the pump beam. With the injection of a p -polarized Gaussian seed beam with an optimal delay, the coherent signal is amplified by nearly three orders of magnitude. The amplified signal is also an OV with the same OAM. This indicates that the vortex pump beam transfers the spatial spiral phase to the N_2^+ gain medium, and the Gaussian

seed beam picks up the spatial spiral phase and is then amplified into an OV. In the presence of the seed beam, we change the vortex pump beam to a CVB pump beam. Interestingly, regardless of whether the polarization state of the seed beam is linear, elliptical, or circular, the amplified signal will always maintain the same CVB mode as the pump beam. We numerically solve three-dimensional coupled wave equations and show how a Gaussian beam eventually evolves into a CVB mode in a cylindrically symmetric gain medium.

Results

Vortex N_2^+ air lasing. The schematic of the experiment is depicted in Fig. 1 (see Methods for more details of the experimental setup). We utilize a SPP to transform p -polarized intense femtosecond laser pulses at 800 nm into an OV with a topological charge of $\ell = 1$ (photon's OAM is $\ell\hbar$). As shown in Fig. 1a, the OV is used as the pump beam to ionize N_2 molecules. The ionization occurs in a laser plasma filament when the pump beam is focused by a lens with a focal length of 30 cm. Nitrogen molecules are mainly ionized into three electronic states of N_2^+ . As shown in the left inset of Fig. 1a, the three states constitute a V-type three-level system consisting of $X^2\Sigma_g^+$, $A^2\Pi_u$ and $B^2\Sigma_u^+$ states.

The spectrum of the detected signal is plotted in the right inset of Fig. 1a, represented by the black line. The signal is identified as coherent radiation of N_2^+ air lasing at 391 nm, which is emitted by the transition of $B^2\Sigma_u^+(v' = 0) \rightarrow X^2\Sigma_g^+(v = 0)$ and includes the P branch (rotation transition: $J \rightarrow J + 1$) and the R branch (rotation transition: $J \rightarrow J - 1$). The beam profile of the signal is a doughnut-type and is recorded by a charge-coupled device (CCD), as shown in Fig. 2b. The signal has the same p -polarized electric field as the pump beam at each spatial point. The singularity at the beam center originates from the helical phase structure. To measure the topological charge of the signal, we employ momentum space mapping of a cylindrical lens⁴⁸ which is schematically depicted in Fig. 2a. The pattern of twisted light at the focus of a cylindrical lens is OAM-dependent. The simulated images at the focal plane of a cylindrical lens are illustrated in Fig. 2f, in which the OVs become deformed patterns with $\ell + 1$ skew bright stripes. Two adjacent bright stripes constitute a deformed vortex core, and the number of the cores is equal to the topological charge. The signal beam is focused experimentally using a cylindrical lens with a focal length of 1 m. As shown in Fig. 2c, the corresponding focal image is a pattern with two bright stripes. Rotating the azimuthal angle of cylindrical lens, we find the number of stripes is always 2. Compared to the simulation results, it is evident that the signal beam is an OV with a topological charge of $\ell = 1$. This implies that the spatial phase structure of the pump beam has been entirely imprinted on the coherent signal of N_2^+ at 391 nm.

With the injection of a p -polarized Gaussian seed beam at an optimal delay (the seed beam has a central wavelength of 400 nm and a spectrum covering 391 nm), the intensity of the signal is amplified, as shown in Fig. 1b. The amplified signal is nearly three orders of magnitude stronger than the unseeded signal. The spectrum of the amplified signal is represented by the black line in the right inset of Fig. 1b. As shown in Fig. 2d, the intensity distribution of the amplified signal also has a doughnut shape. Similarly, the amplified signal beam is focused by the cylindrical lens and the focal image is illustrated in Fig. 2e. This reveals that the amplified signal also has the same topological charge as that of the pump beam. However, in the theory of superfluorescence, it is commonly regarded that if an external seed is injected, it will dominate the establishment of macroscopic polarization. Theoretically, the spatial phase distribution of the amplified signal

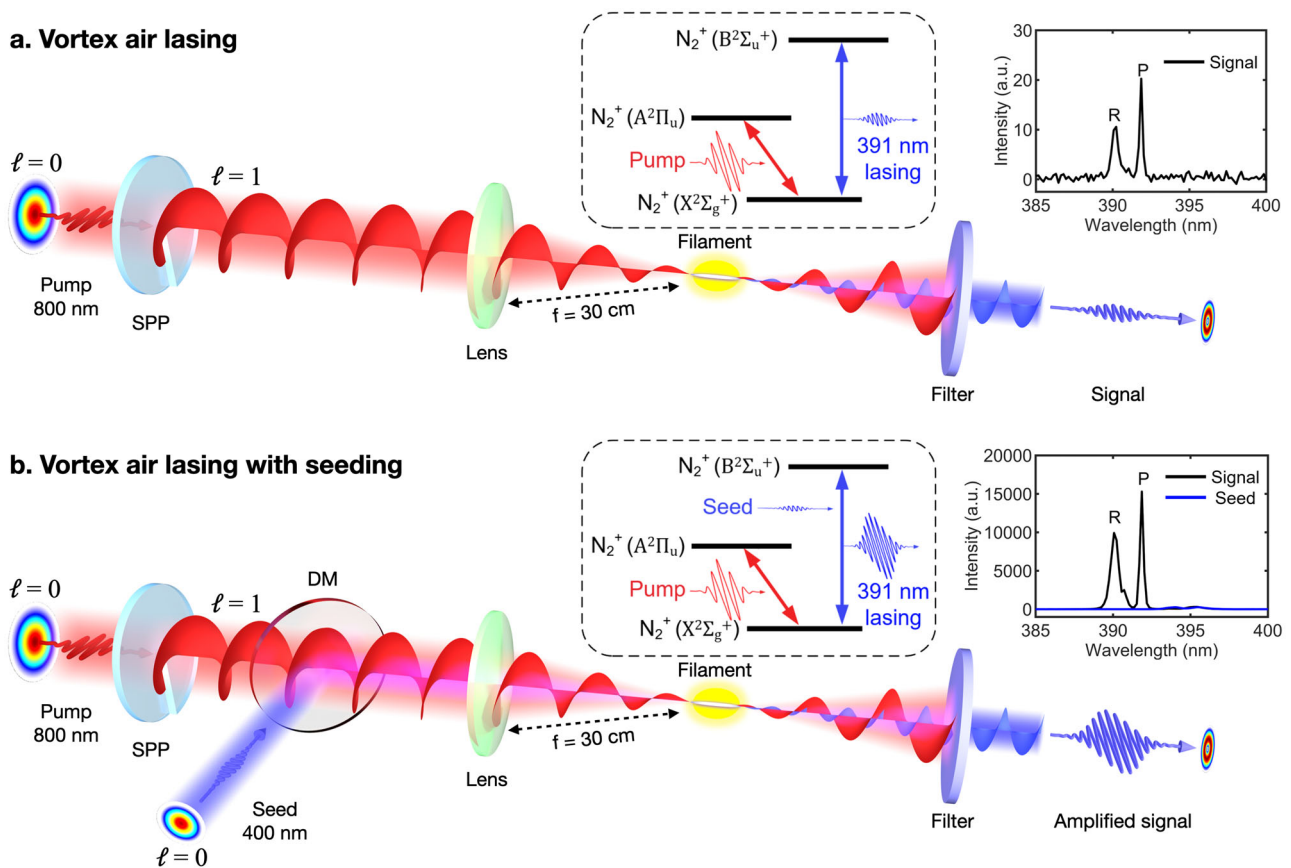


Fig. 1 Schematic of the experiment. Layout diagramming the generation processes of vortex air lasing of N_2^+ without seeding (**a**) and with seeding (**b**). **a** An intense vortex beam at 800 nm is used to pump N_2 molecules alone. **b** An intense vortex beam at 800 nm is used to pump N_2 molecules and a weak Gaussian beam with a spectrum covering 391 nm is injected to stimulate excited N_2^+ ions. Left insets surrounded by dash lines: schematics of the three-level system of N_2^+ air lasing at 391 nm without seeding (**a**) and with seeding (**b**). Right insets: spectra of (**a**) the signal of N_2^+ air lasing; (**b**) the amplified signal of N_2^+ air lasing and the seed light. DM dichroic mirror, SPP spiral phase plate.

should be independent of that of the vortex pump beam. Interestingly, our results indicate that the spatial phase of the pump beam is simultaneously transferred to the amplified signal via the N_2^+ gain medium, which points to an unrevealed physical mechanism in N_2^+ air lasing in addition to the current superfluorescence theory.

Vector N_2^+ air lasing. Inspired by the results of OVVs with seeding, we replace the SPP with an SWP to change the pump beam into a CVB. The azimuthal angle of the SWP is rotated to let the pump beam become radially polarized. In the same way, the p -polarized Gaussian seed beam is injected into the plasma filament with an optimal delay, and then an amplified signal of N_2^+ air lasing at 391 nm is observed. As shown in the first panel of Fig. 3a, the intensity distribution of the amplified signal is also a doughnut-shaped pattern. In contrast to OVVs, spatially variant polarization states contribute to the singularity here. A polarizer is placed in front of the CCD to observe the spatial polarization distribution. The three panels on the right in Fig. 3a show the intensity distributions of the amplified air lasing after passing through the polarizer with different polarization axis angles, i.e., 0° , 45° , and 90° . As can be seen, if filtered by a polarizer, the intensity distribution of the amplified signal beam will appear as two lobes that rotate with the polarization axis angle of the polarizer. The intensity distributions in the second and third panels possess the features of HG_{01} and HG_{10} modes, respectively (HG modes, Hermit-Gaussian modes⁴⁹). It is well known that a radially polarized beam can be expressed as a coherent

superposition of p -polarized HG_{01} and s -polarized HG_{10} modes⁴. The results show that the amplified signal exhibits the characteristics of a radially polarized mode, which is identical to that of the pump beam. We then change the seed beam into elliptically and circularly polarized states in turn (the ellipticities are 0.73 and 0.92, respectively), and the corresponding results have the same characteristic of the radially polarized mode, as shown in Fig. 3b and Fig. 3c. It is obvious that the polarization state of the amplified signal is completely dictated by the vector pump beam and is independent of the Gaussian seed beam.

For further confirmation, we rotate the SWP to allow the pump beam to become azimuthally polarized. Similar to the results shown in Fig. 3, regardless of whether the seed beam is linearly, elliptically, or circularly polarized, the corresponding amplified signals always possess the feature of the azimuthally polarized mode, as shown in Fig. 4. Moreover, if the pump beam is in any CVB mode that is between the radially and azimuthally polarized modes, the amplified signal will also possess the same CVB mode as the pump beam. Therefore, a CVB mode tuning of N_2^+ air lasing can be simply implemented. We also observed a series of beam profiles at different time delays between the pump and the seed, that is, 0.1, 0.2, 0.3, 0.4, and 0.5 ps. We found that the intensity depends on the delay while the profile keeps CVB mode unchanged.

Discussion

To interpret how a Gaussian beam can be amplified into a CVB, we build a theoretical model of a cylindrically symmetric gain

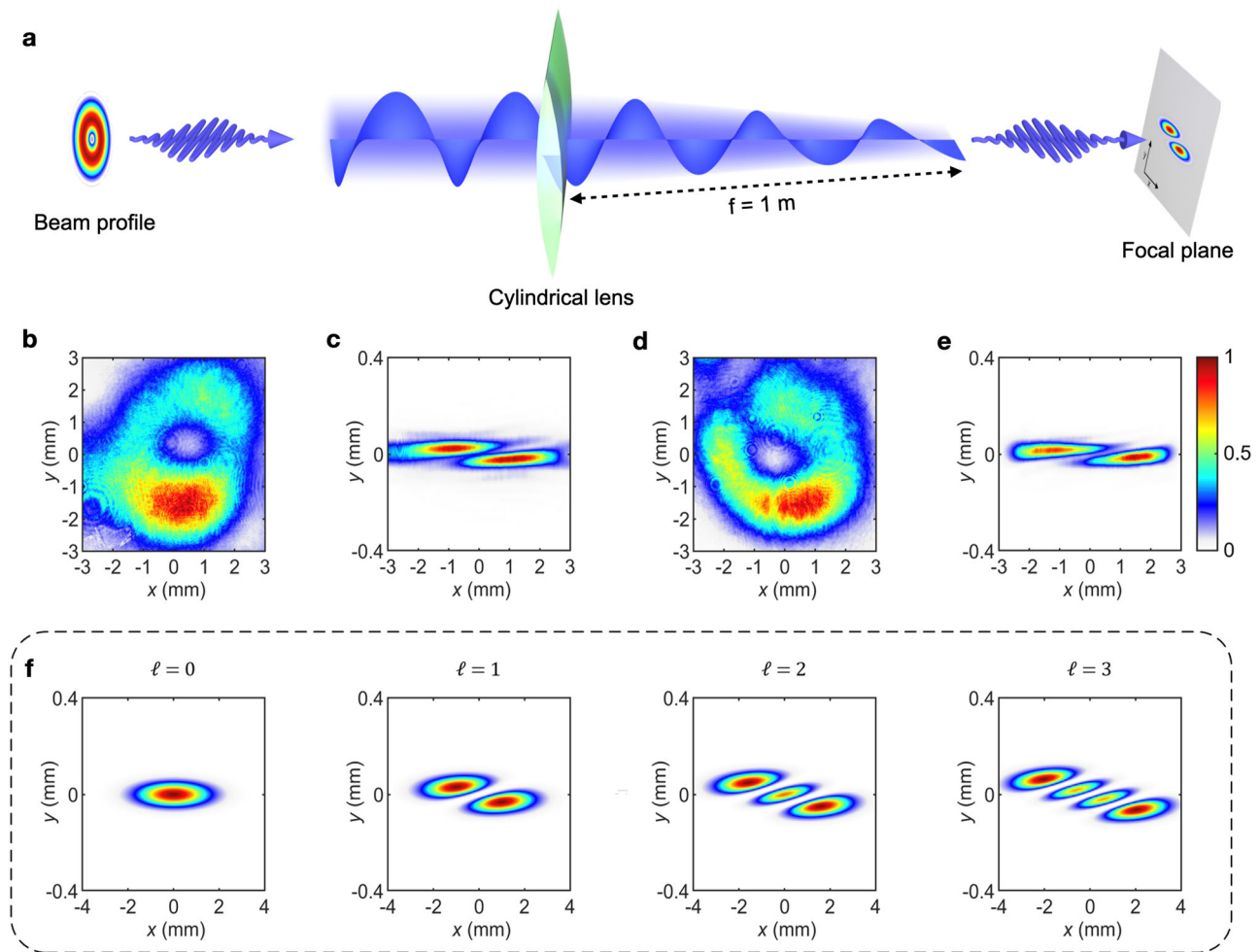


Fig. 2 Intensity distributions and focal images of N_2^+ lasing at 391 nm pumped by OVVs. **a** Schematic of the momentum space mapping of a cylindrical lens. **b, c** The measured intensity distribution and focal image of N_2^+ air lasing at 391 nm without seeding. **d, e** The measured intensity distribution and focal image of N_2^+ air lasing at 391 nm with seeding. **f** Simulated focal images of vortex beams with different topological charges, that is 0, 1, 2, and 3, respectively. All beams are focused in the y direction by the cylindrical lens. The focal length of the cylindrical lens is 1 m in both experiments and calculations. The number of experimentally observed strippers is always two in all directions.

medium. In previous experiments, the polarization states of the pump beams and seed beams are usually linearly polarized and synergistically determine the polarization direction of the amplified signal⁵⁰. The amplified signal is linearly polarized, and the polarization direction is between the pump and seed beams. Moreover, the intensity of the amplified signal is dependent on the angle between the polarization directions of the pump and seed beams. When the angle is 0° , the amplification ratio is maximum⁵¹. It decreases as the angle increases, until it reaches a minimum when the angle is 90° . These imply that the maximum and minimum gain directions are parallel and perpendicular to the polarization direction of the pump beam, respectively. We believe that this is caused by the average alignment of N_2^+ induced by the pump beams. First, the pump beams align the nitrogen molecules along the laser polarization direction before and after the ionization. In addition, the optimal ionization direction of the highest occupied molecular orbital (HOMO) and HOMO-2 of N_2 is parallel to the molecular axis⁵². If N_2 molecules eject an outer valence electron in HOMO or HOMO-2, they will become N_2^+ ions in the state of $X^2\Sigma_g^+$ or $B^2\Sigma_u^+$ ⁵³. These two factors result in most of the N_2^+ ions in the states $X^2\Sigma_g^+$ and $B^2\Sigma_u^+$ being permanently aligned along the polarization direction of the pump beams⁵⁴. Because the transition dipole moment between $X^2\Sigma_g^+$ and $B^2\Sigma_u^+$ is also parallel to the molecular axis, the

electric field component of the seed beam parallel to the polarization direction of the pump beam has the maximum amplification, and the component perpendicular to the polarization direction of the pump beam has the minimum amplification.

Consequently, if the pump beams are radially (azimuthally) polarized, the maximum gain direction of the N_2^+ medium will present a radial (azimuthal) distribution in the filament; hence, the minimum gain direction will be azimuthal (radial). Based on this, we build a theoretical model of the medium with a cylindrically symmetric gain, which is described by two three-dimensional coupled wave equations (see Methods for details of the model). In this model, we focus on how the signal spatially evolves from a Gaussian mode into a CVB mode in an anisotropic gain medium. Thus, the time dependence of the population distribution in the ground and excited states of N_2^+ is neglected, i.e., the amplification term is deemed as a constant in the calculations. The effect of the photoinduced refractive index change can also be ignored, because it has no impact on the cylindrical symmetry of the results.

The numerical results of the theoretical model are shown in Fig. 5. This shows an evolution process in which a p -polarized Gaussian seed beam gradually becomes a radially polarized beam as it propagates in a radial gain medium. When the propagation

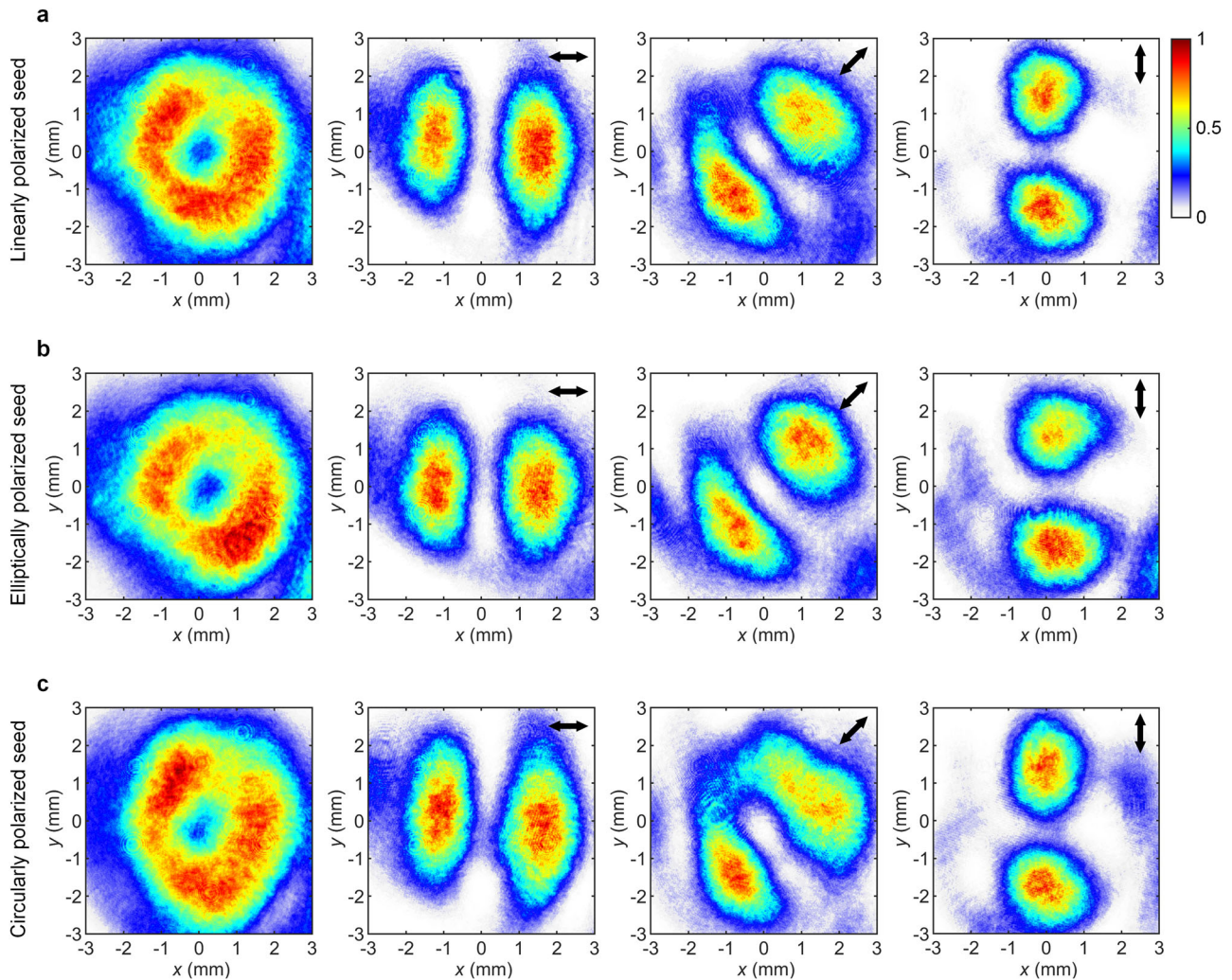


Fig. 3 Intensity distributions of N_2^+ lasing at 391 nm pumped by radially polarized CVBs with seeding. **a–c** The polarization states of seed beams are linearly, elliptically, and circularly polarized, respectively. The panels in the first column show the intensity distributions of signals directly recorded by the CCD. The three columns on the right show the intensity distributions filtered by a polarizer with different angles, i.e., 0° , 45° , and 90° . The intensity distributions of each row are normalized by the same standard as the first panel. The black arrows indicate the polarization axis direction of the polarizer.

distance is 0 mm, as shown in Fig. 5a, the y component of the intensity is null, and the intensity distribution, $|E|^2$, is identical to its x component, $|E_x|^2$. As the propagation distance increases shown in Fig. 5b, both the intensity of the light field and the ratio of the y component to the x component increase. At the exit of the gain medium, the seed beam has been amplified thousands of times and eventually becomes radially polarized, as shown in Fig. 5c. Similarly, if the gain distribution of the medium is azimuthal, the p -polarized seed beam will be amplified into an azimuthally polarized beam (see Fig. S3 in Supplementary Note 2 of Supplementary Information). The model is applicable to any polarization state of the seed beam. We simulate the injection of a circularly polarized seed beam, which is also amplified into a CVB (see Figs. S4, S5 in Supplementary Note 2 of Supplementary Information). The experimental results are well reproduced in the simulations.

Generally, the cylindrically symmetric gain medium supports a feasible way in which one component of the electric field can be amplified to that is orthogonal to it, namely, the E_y can be amplified from the E_x . However, the anisotropic gain medium cannot provide an abrupt transverse phase difference of π between the centrosymmetric points for the formation of a CVB when it is seeded by a Gaussian beam. Interestingly, the transfer

of the spatial phase from the pump beam to the amplified signal can compensate for the phase difference, i.e., in the case of vector results, the phase structure of CVBs is also transferred to the amplified signal, which is consistent with the vortex results. In the calculations, we treat the phase-transfer problem by imposing the spatial phase of the pump beam on the seed beam at the entrance of the gain medium. The numerical results demonstrate that a weak Gaussian seeding beam can evolve into a strong CVB during the propagation of a medium with a cylindrically symmetric distribution of gain, which strongly supports our physical explanation.

In air lasing using a vortex pump beam without seeding, the coherent signal of N_2^+ air lasing at 391 nm inherits the spiral phase structure of the vortex pump beam. This is consistent with the previous understanding that N_2^+ air lasing at 391 nm is self-seeded by the white light originating from the supercontinuum of the pump beam. The supercontinuum in the filament extends the spectrum of the pump beam from the infrared region to the ultraviolet region as a result of self-phase modulation⁵⁵, which naturally brings the helical phase structure of the pump light to the white light without changing OAM^{56,57}. It should be noted that the vortex 391 lasing is distinct from the vortex HHG^{26,27,58} and other nonlinear parametric processes²⁵ in which light

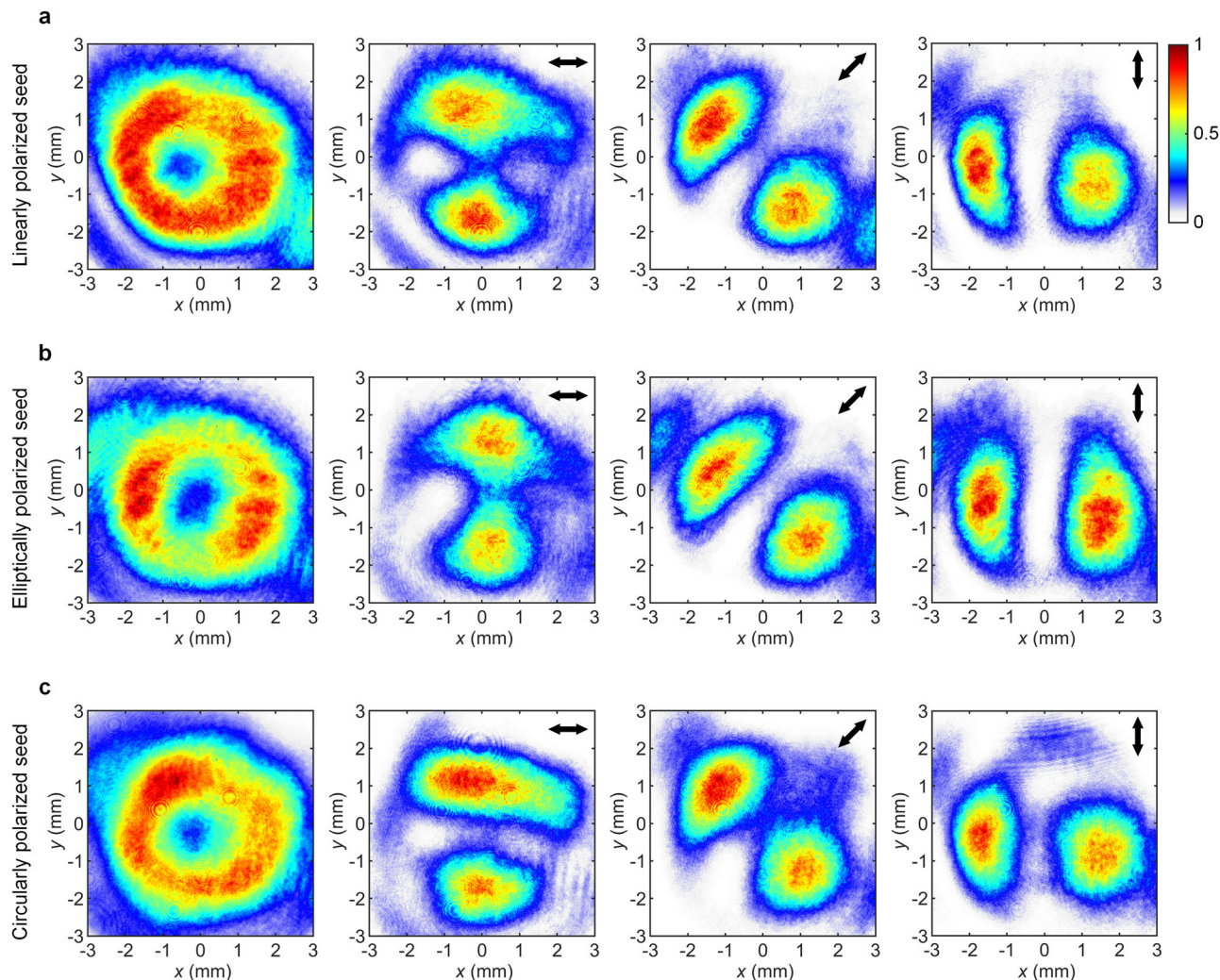


Fig. 4 Intensity distributions of N_2^+ lasing at 391 nm pumped by azimuthally polarized CVBs with seeding. **a–c** The polarization states of seed beams are linearly, elliptically, and circularly polarized, respectively. The panels in the first column show the intensity distributions of signals directly recorded by the CCD. The three columns on the right show the intensity distributions filtered by a polarizer with different angles, i.e., 0° , 45° , and 90° , respectively. The intensity distributions of each row are normalized by the same standard as the first panel. The black arrows indicate the polarization axis direction of the polarizer.

interacts with matter without changing the quantum state of the material. Consequently, these nonlinear processes satisfy the conservations of energy and angular momentum, where the corresponding selection rules must follow the conservations and then the frequency and OAM of the n th harmonic are n times those of the pump light.

When seeding with a Gaussian beam, the coherent signal is amplified and still has the same topological charge as the pump beam. One may expect that, in the current theory of superfluorescence, the spatial phase information of the pump beam will be lost in the amplified signal under the V-type three-level system because it is generally considered that the macroscopic polarization of the N_2^+ medium is predominantly induced by the external seed beam. Theoretically, the spatial phase distribution of the amplified signal should be the same as that of the Gaussian seed beam. Interestingly, the spatial spiral phase of the pump beam is eventually transferred to the amplified signal of N_2^+ air lasing at 391 nm, namely, the OAM of the pump beam is transferred to the amplified signal via N_2^+ medium in the laser filamentation. This manifests that there is an unrevealed physical mechanism in N_2^+ air lasing in addition to the current superfluorescence theory, which needs to be further studied.

If pumping with a CVB in the presence of seeding, the Gaussian seed beam is correspondingly amplified into a CVB. The polarization state of the amplified signal is completely determined by the vector pump beam. Regardless of whether the seed beam is linearly, elliptically, or circularly polarized, the amplified signal will always be a CVB with an identical mode as the pump beam. The vector results with seeding are different from previous experimental results, where the pump and seed beams are both linearly polarized⁵⁰. In the previous cases, the pump and seed beams synergistically control the polarization direction of the amplified signal. Consequently, the amplified signal is linearly polarized, and the polarization direction is between the pump and seed beams. These two different phenomena both originate from the laser alignment of N_2^+ induced by the pump beam, i.e., the laser alignment determines the spatial feature of maximum gain direction of N_2^+ medium. While a p -polarized pump beam produces an N_2^+ medium with a horizontal maximum gain direction, the maximum gain direction of the N_2^+ medium induced by a CVB exhibits a cylindrical distribution. The vector results suggest that laser-induced alignment could potentially be employed in commercial molecular lasers to generate high-power CVBs or other kinds of VBs.

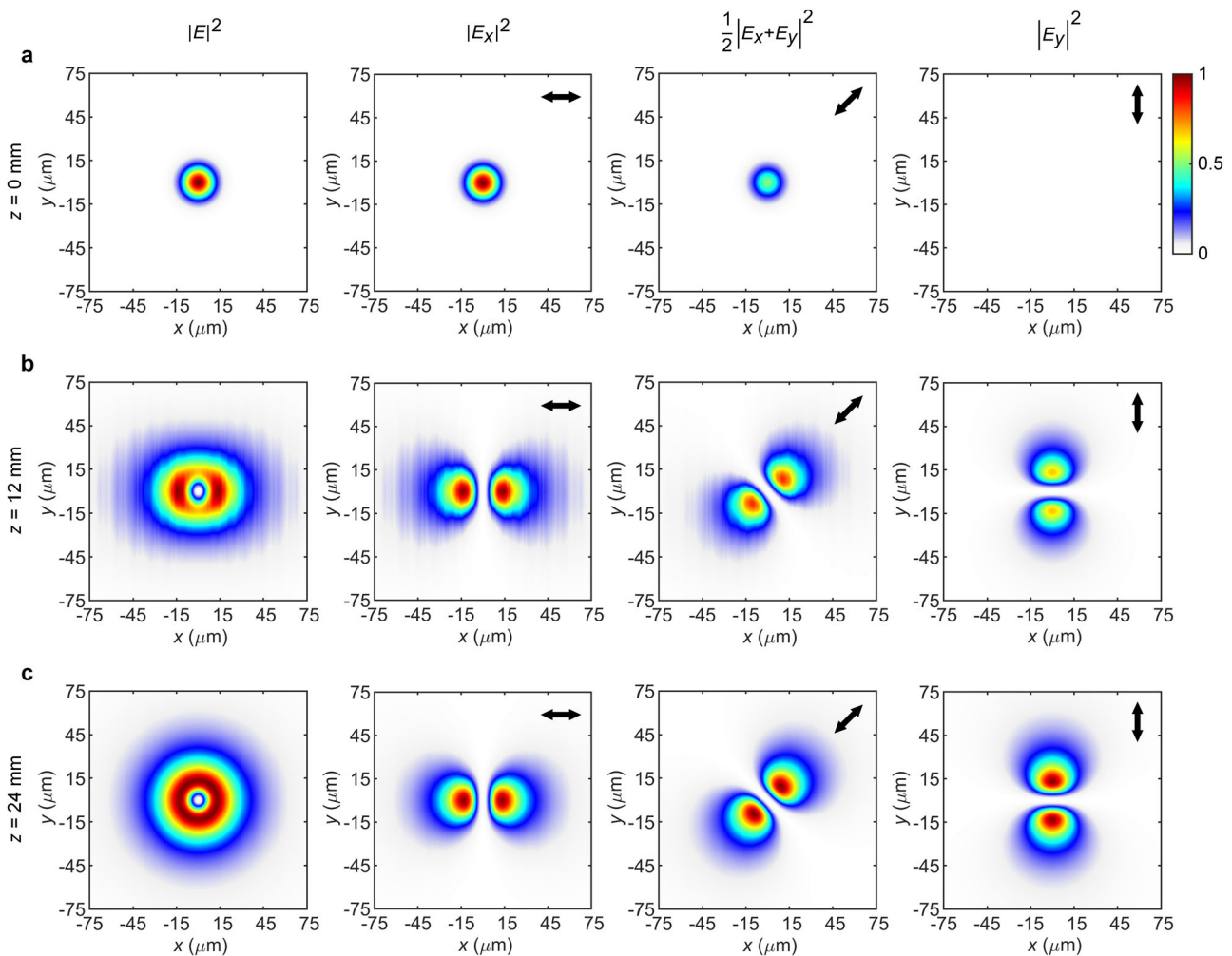


Fig. 5 Simulated intensity distributions in a radial gain medium. **a–c** Simulated intensity distributions at different distances in the gain medium, that is, 0 mm, 12 mm, and 24 mm, respectively. The seed light is linearly polarized. The amplification ratios are about 1 (**a**), 154 (**b**), and 6647 (**c**) times, respectively. The intensity distributions of each row are normalized by the same standard as the first panel. The black arrows indicate the directions of polarization components.

In conclusion, we report the first implementation of structured air lasing. We have experimentally generated two typical types of structured light by N_2^+ air lasing, that is, OV and CVB. We find that the OV at 800 nm transfers the spatial spiral phase to the N_2^+ gain medium, and the seed beam picks up the spatial spiral phase and is then amplified into a vortex beam at 391 nm. To the best of our knowledge, this phase transfer from the pump beam to the seed beam in N_2^+ air lasing has not been identified before, and its underlying mechanism is an intriguing direction for further investigation. The CVB at 800 nm aligns the nitrogen ions along its polarization direction, producing a cylindrically symmetric gain medium of N_2^+ . This anisotropic gain medium allows for the amplification of a seed beam with any spatially homogeneous polarization states into a CVB. From a technical perspective, this work provides a promising approach to generating structured light, in which a Gaussian beam can be directly amplified into structured light by cavity-free lasing action instead of a complicated optical system.

Methods

Experimental details. The p -polarized Gaussian laser pulses at a central wavelength of 800 nm are launched from a regenerate amplification system of a Ti:Sapphire laser, which delivers 35 fs pulses at a repetition frequency of 1 kHz. The laser pulses are then split into two beam paths. The first one is used as a pump beam with a single-

pulse energy of 1.8 mJ. The energy is adjusted by a half-wave plate and a polarizer. First, an SPP is placed in the beam path to transform the pump beam into a vortex beam (the topological charge is $\ell = 1$). Then, we turn the pump beam into a CVB by replacing the spiral phase plate with an SWP. By rotating the azimuthal angle of the SWP, the CVB mode can be continuously tuned from radial polarization to azimuthal polarization. The second path passes through a half-wave plate and a 0.1-mm-thick beta-barium borate crystal (BBO) to produce a p -polarized seed beam with a central wavelength of 400 nm, a spectrum covering 391 nm and a single-pulse energy of about several nanojoules. A quarter-wave plate is utilized to change the polarization state of the seed beam (linear, elliptical, or circular polarization). The pump and the seed beams are combined collinearly by a dichroic mirror (DM) with high reflectivity around 400 nm and high transmission around 800 nm. In this experiment setup, the DM also plays the role of filter to remove the second harmonic of the pump light generated from waveplates. Otherwise, the second harmonic mixed in the pump light will serve as an external seed light that carries second order of OAM, which decrease the mode purity of the output signal. The two beams are focused collinearly into a gas chamber using a lens with a focal length of 30 cm and a single filament is produced. The chamber is filled with pure N_2 gas at 30 mbar. The pump beam is filtered out by a 650 nm short filter and three bandpass 390 ± 5 nm bandpass filters before signal detection. The lasing emission of N_2^+ at 391 nm is collected by a fiber head connected to a grating spectrometer or recorded by a CCD.

The output mode is sensitive to the quality of the laser filament. In the experiment, many factors are detrimental to the filament quality, such as the chromatic aberration of the focusing lens, the spatial nonuniformity of the pump light, the center deviation and the chromatic dispersion of the SWP. The above factors make it not trivial to obtain a signal with a good doughnut-type profile for both OV and CVB, and a good cylindrical symmetric polarization distribution for CVB. By careful and systematic optimization of the experimental conditions, we finally obtained a good output mode as the main text presents.

Theoretical model. The three-dimensional coupled wave equations of the medium with radial gain (under the condition of a slowly varying approximation) are expressed as

$$\frac{\partial^2 E_x}{\partial x^2} + \frac{\partial^2 E_x}{\partial y^2} + 2ik \frac{\partial E_x}{\partial z} = -\mu\omega^2 P_x, \quad (1)$$

and

$$\frac{\partial^2 E_y}{\partial x^2} + \frac{\partial^2 E_y}{\partial y^2} + 2ik \frac{\partial E_y}{\partial z} = -\mu\omega^2 P_y, \quad (2)$$

where E_x and E_y are the x and y components of the slowly varying amplitude of the electric field, respectively, k is the wave number of the electric field, ω is the angular frequency of the electric field, μ is the permeability, P_x and P_y are the x and y components of the slowly varying part of the medium macroscopic polarization, respectively. The macroscopic polarization is the functions of both E_x and E_y , namely,

$$P_x = C \langle \cos^2 \theta \rangle (E_x \cos^2 \varphi + E_y \sin \varphi \cos \varphi) + C \langle \sin^2 \theta \rangle (E_x \sin^2 \varphi - E_y \sin \varphi \cos \varphi), \quad (3)$$

$$P_y = C \langle \cos^2 \theta \rangle (E_x \sin \varphi \cos \varphi + E_y \sin^2 \varphi) - C \langle \sin^2 \theta \rangle (E_x \sin \varphi \cos \varphi - E_y \cos^2 \varphi). \quad (4)$$

The parameter C is given by

$$C = -\frac{i}{\hbar\gamma} d_{BK}^2 N (\rho_{22} - \rho_{11}), \quad (5)$$

where \hbar is the reduced Planck constant, γ is the decay rate, d_{BK} is the transition dipole moment between $X^2\Sigma_g^+$ and $B^2\Sigma_u^+$ states, N represents the average number of particles per unit volume, ρ_{11} and ρ_{22} are the probabilities of being in the upper and lower states, respectively, $N(\rho_{22} - \rho_{11})$ represents the difference in the population of the upper and lower states per unit volume that is determined by the intensity of pump light and characterizes the amplification, φ is the azimuth of the xy plane, and $\langle \cos^2 \theta \rangle$ and $\langle \sin^2 \theta \rangle$ are the average alignment degrees of N_2^+ that are parallel and perpendicular to the polarization direction of the pump beam, respectively (see Equation S1–S11 in Supplementary Note 1 of Supplementary Information for details of derivation). The equations are solved using the split-step Fourier method. In the calculations, the time dependence of the population distribution in the ground and the excited states is neglected, namely, ρ_{22} and ρ_{11} are regarded as constants. The waists of the seed beam and the gain medium (plasma filament) are both set to 15 μm . The cross-section of the gain medium is set as the LG mode with $\ell=1$ (because the intensity distribution of CVBs has the same pattern as that of the OV with $\ell=1$). The ratio of $\langle \cos^2 \theta \rangle$ to $\langle \sin^2 \theta \rangle$ is set to 2. The length of the gain medium is set to 24 mm, which is close to the length of the laser filament in the experiment. The parameter C is set to make the seed light amplified around 8000 times, which is comparable to the experimental results. If the gain distribution is azimuthal, then $\langle \cos^2 \theta \rangle$ and $\langle \sin^2 \theta \rangle$ will exchange with each other in the equations.

Data availability

The data that support the findings presented in the main text are available from the corresponding author upon reasonable request.

Code availability

The codes that support the simulations presented in the main text and the Supplementary Information are available from the corresponding author upon reasonable request.

Received: 31 December 2022; Accepted: 27 April 2023;

Published online: 09 May 2023

References

- Forbes, A., de Oliveira, M. & Dennis, M. R. Structured light. *Nat. Photon.* **15**, 253–262 (2021).
- Rubinsztein-Dunlop, H. et al. Roadmap on structured light. *J. Opt.* **19**, 013001 (2017).
- Shen, Y. et al. Optical vortices 30 years on: OAM manipulation from topological charge to multiple singularities. *Light Sci. Appl.* **8**, 90 (2019).
- Zhan, Q. Cylindrical vector beams: from mathematical concepts to applications. *Adv. Opt. Photon.* **1**, 1–57 (2009).
- Allen, L., Beijersbergen, M. W., Spreeuw, R. J. C. & Woerdman, J. P. Orbital angular momentum of light and the transformation of Laguerre-Gaussian laser modes. *Phys. Rev. A* **45**, 8185–8189 (1992).
- Vicidomini, G., Bianchini, P. & Diaspro, A. STED super-resolved microscopy. *Nat. Methods* **15**, 173–182 (2018).
- Grier, D. G. A revolution in optical manipulation. *Nature* **424**, 810–816 (2003).
- Padgett, M. & Bowman, R. Tweezers with a twist. *Nat. Photon.* **5**, 343–348 (2011).
- Lavery, M. P. J., Speirits, F. C., Barnett, S. M. & Padgett, M. J. Detection of a spinning object using light's orbital angular momentum. *Science* **341**, 537–540 (2013).
- Wang, J. et al. Terabit free-space data transmission employing orbital angular momentum multiplexing. *Nat. Photon.* **6**, 488–496 (2012).
- Ren, H., Li, X., Zhang, Q. & Gu, M. On-chip noninterference angular momentum multiplexing of broadband light. *Science* **352**, 805–809 (2016).
- Moradi, H., Shahabadi, V., Madadi, E., Karimi, E. & Hajizadeh, F. Efficient optical trapping with cylindrical vector beams. *Opt. Express* **27**, 7266–7276 (2019).
- Chen, R., Agarwal, K., Sheppard, C. J. R. & Chen, X. Imaging using cylindrical vector beams in a high-numerical-aperture microscopy system. *Opt. Lett.* **38**, 3111–3114 (2013).
- Neugebauer, M., Woźniak, P., Bag, A., Leuchs, G. & Banzer, P. Polarization-controlled directional scattering for nanoscopic position sensing. *Nat. Commun.* **7**, 11286 (2016).
- Wang, J. Advances in communications using optical vortices. *Photon. Res.* **4**, B14–B28 (2016).
- Ndagano, B. et al. Characterizing quantum channels with non-separable states of classical light. *Nat. Phys.* **13**, 397–402 (2017).
- Parigi, V. et al. Storage and retrieval of vector beams of light in a multiple-degree-of-freedom quantum memory. *Nat. Commun.* **6**, 7706 (2015).
- Fang, Y. et al. Photoelectronic mapping of the spin-orbit interaction of intense light fields. *Nat. Photon.* **15**, 115–120 (2021).
- Stav, T. et al. Quantum entanglement of the spin and orbital angular momentum of photons using metamaterials. *Science* **361**, 1101–1104 (2018).
- Beijersbergen, M., Coerwinkel, R., Kristensen, M. & Woerdman, J. Helical-wavefront laser beams produced with a spiral phaseplate. *Opt. Commun.* **112**, 321–327 (1994).
- Naidoo, D. et al. Controlled generation of higher-order Poincaré sphere beams from a laser. *Nat. Photon.* **10**, 327–332 (2016).
- Liu, S. et al. Highly efficient generation of arbitrary vector beams with tunable polarization, phase, and amplitude. *Photon. Res.* **6**, 228–233 (2018).
- Ngcobo, S., Litvin, I., Burger, L. & Forbes, A. A digital laser for on-demand laser modes. *Nat. Commun.* **4**, 2289 (2013).
- Forbes, A. Structured light from lasers. *Laser Photon. Rev.* **13**, 1900140 (2019).
- Buono, W. T. & Forbes, A. Nonlinear optics with structured light. *Opto-Electron. Adv.* **5**, 210174 (2022).
- Gariepy, G. et al. (2014). Creating high-harmonic beams with controlled orbital angular momentum. *Phys. Rev. Lett.* **113**, 153901 (2014).
- Rego, L. et al. Generation of extreme-ultraviolet beams with time-varying orbital angular momentum. *Science* **364**, eaaw9486 (2019).
- Hernández-García, C. et al. Extreme ultraviolet vector beams driven by infrared lasers. *Optica* **4**, 520–526 (2017).
- Dorney, K. M. et al. Controlling the polarization and vortex charge of attosecond high-harmonic beams via simultaneous spin-orbit momentum conservation. *Nat. Photon.* **13**, 123–130 (2019).
- Dogariu, A., Michael, J. B., Scully, M. O. & Miles, R. B. High-gain backward lasing in air. *Science* **331**, 442–445 (2011).
- Yao, J. et al. High-brightness switchable multiwavelength remote laser in air. *Phys. Rev. A* **84**, 051802 (2011).
- Xu, H., Lötstedt, E., Iwasaki, A. & Yamanouchi, K. Sub-10-fs population inversion in N_2^+ in air lasing through multiple state coupling. *Nat. Commun.* **6**, 8347 (2015).
- Yao, J. et al. Population redistribution among multiple electronic states of molecular nitrogen ions in strong laser fields. *Phys. Rev. Lett.* **116**, 143007 (2016).
- Liu, Y. et al. Unexpected sensitivity of nitrogen ions superradiant emission on pump laser wavelength and duration. *Phys. Rev. Lett.* **119**, 203205 (2017).
- Britton, M. et al. Testing the role of recollision in N_2^+ air lasing. *Phys. Rev. Lett.* **120**, 133208 (2018).
- Zhang, A. et al. Coherent modulation of superradiance from nitrogen ions pumped with femtosecond pulses. *Opt. Express* **27**, 12638–12646 (2019).
- Ando, T. et al. Rotational, vibrational, and electronic modulations in N_2^+ lasing at 391 nm: evidence of coherent $B^2\Sigma_u^+ - X^2\Sigma_g^+ - A^2\Pi_u$ coupling. *Phys. Rev. Lett.* **123**, 203201 (2019).
- Richter, M. et al. Rotational quantum beat lasing without inversion. *Optica* **7**, 586–592 (2020).
- Liu, Y. et al. Recollision-induced superradiance of ionized nitrogen molecules. *Phys. Rev. Lett.* **115**, 133203 (2015).
- Zhang, A. et al. Subfemtosecond-resolved modulation of superfluorescence from ionized nitrogen molecules by 800-nm femtosecond laser pulses. *Opt. Express* **27**, 14922–14930 (2019).

41. Zhang, X. et al. Coherent control of the multiple wavelength lasing of N_2^+ : coherence transfer and beyond. *Optica* **8**, 668–673 (2021).
42. Findik, G. et al. High-temperature superfluorescence in methyl ammonium lead iodide. *Nat. Photon.* **15**, 676–680 (2021).
43. Biliroglu, M. et al. Room-temperature superfluorescence in hybrid perovskites and its origins. *Nat. Photon.* **16**, 324–329 (2022).
44. Huang, K. et al. Room-temperature upconverted superfluorescence. *Nat. Photon.* **16**, 737–742 (2022).
45. Bonifacio, R. & Lugiato, L. A. Cooperative radiation processes in two-level systems: superfluorescence. *Phys. Rev. A* **11**, 1507–1521 (1975).
46. Li, H. et al. Significant enhancement of N_2^+ lasing by polarization-modulated ultrashort laser pulses. *Phys. Rev. Lett.* **122**, 013202 (2019).
47. Li, H. et al. Giant enhancement of air lasing by complete population inversion in N_2^+ . *Phys. Rev. Lett.* **125**, 053201 (2020).
48. Alperin, S. N., Niederriter, R. D., Gopinath, J. T. & Siemens, M. E. Quantitative measurement of the orbital angular momentum of light with a single, stationary lens. *Opt. Lett.* **41**, 5019–5022 (2016).
49. Kogelnik, H. & Li, T. Laser Beams and Resonators. *Appl. Opt.* **5**, 1550–1567 (1966).
50. Xie, H. et al. Role of rotational coherence in femtosecond-pulse-driven nitrogen ion lasing. *Phys. Rev. Res.* **2**, 023329 (2020).
51. Lei, M., Wu, C., Zhang, A., Gong, Q. & Jiang, H. Population inversion in the rotational levels of the superradiant N_2^+ pumped by femtosecond laser pulses. *Opt. Express* **25**, 4535–4541 (2017).
52. Petretti, S., Vanne, Y. V., Saenz, A., Castro, A. & Declève, P. Alignment-dependent ionization of N_2 , O_2 , and CO_2 in intense laser fields. *Phys. Rev. Lett.* **104**, 223001 (2010).
53. Becker, A., Bandrauk, A. D. & Chin, S. L. S-matrix analysis of non-resonant multiphoton ionisation of inner-valence electrons of the nitrogen molecule. *Chem. Phys. Lett.* **343**, 345–350 (2001).
54. Pavičić, D., Lee, K. F., Rayner, D. M., Corkum, P. B. & Villeneuve, D. M. Direct measurement of the angular dependence of ionization for N_2 , O_2 , and CO_2 in intense laser fields. *Phys. Rev. Lett.* **98**, 243001 (2007).
55. Bergé, L., Skupin, S., Nuter, R., Kasparian, J. & Wolf, J. P. Ultrashort filaments of light in weakly ionized, optically transparent media. *Rep. Prog. Phys.* **70**, 1633–1713 (2007).
56. Tokizane, Y., Oka, K. & Morita, R. Supercontinuum optical vortex pulse generation without spatial or topological-charge dispersion. *Opt. Express* **17**, 14517–14525 (2009).
57. Li, D. et al. Powerful supercontinuum vortices generated by femtosecond vortex beams with thin plates. *Photon. Res.* **10**, 802–809 (2022).
58. Kong, F. et al. Controlling the orbital angular momentum of highharmonic vortices. *Nat. Commun.* **8**, 14970 (2017).

Acknowledgements

This work is supported by the National Key R&D Program of China (Grant No. 2018YFB2200401), and the National Natural Science Foundation of China (Grants

Nos. 41527807, 12034013). The authors thank Jiahao Dong for his assistance in figure design.

Author contributions

J.G. performed the experiments with the assistance of X.Z., Y.W., and Q.L. J.G., Yi L., Yunquan L., and H.J. analyzed the data. H.J. gave the theoretical explanation and guided J.G. to build the model. J.G. performed the simulations and drafted the paper. Yi L., Yunquan L., and H.J. supervised the project and guided the development of the paper. Yi L. and C.W. provided elements of the experimental setup. Y.F., Z.L., and Q.G. participated in discussions. All authors approved the final version of the paper.

Competing interests

The authors declare no competing interests.

Additional information

Supplementary information The online version contains supplementary material available at <https://doi.org/10.1038/s42005-023-01226-9>.

Correspondence and requests for materials should be addressed to Yi Liu, Yunquan Liu or Hongbing Jiang.

Peer review information *Communications Physics* thanks Andrew Forbes and the other, anonymous, reviewer(s) for their contribution to the peer review of this work. Peer reviewer reports are available.

Reprints and permission information is available at <http://www.nature.com/reprints>

Publisher's note Springer Nature remains neutral with regard to jurisdictional claims in published maps and institutional affiliations.



Open Access This article is licensed under a Creative Commons Attribution 4.0 International License, which permits use, sharing, adaptation, distribution and reproduction in any medium or format, as long as you give appropriate credit to the original author(s) and the source, provide a link to the Creative Commons license, and indicate if changes were made. The images or other third party material in this article are included in the article's Creative Commons license, unless indicated otherwise in a credit line to the material. If material is not included in the article's Creative Commons license and your intended use is not permitted by statutory regulation or exceeds the permitted use, you will need to obtain permission directly from the copyright holder. To view a copy of this license, visit <http://creativecommons.org/licenses/by/4.0/>.

© The Author(s) 2023